

Photons from neutrinos: the gamma ray echo of a supernova neutrino burst

CECILIA LUNARDINI ¹, JOSHUA LOEFFLER,¹ MAINAK MUKHOPADHYAY ², MATTHEW J. HURLEY ³,
EBRAHEEM FARAG ^{4,5} AND F.X. TIMMES ⁴

¹*Department of Physics, Arizona State University, Tempe, AZ 85287-1504 USA*

²*Department of Physics; Department of Astronomy & Astrophysics; Center for Multimessenger Astrophysics, Institute for Gravitation and the Cosmos, The Pennsylvania State University, University Park, PA 16802, USA*

³*Department of Physics, Stanford University, Stanford, California 94305, USA*

⁴*School of Earth and Space Exploration, Arizona State University, Tempe, AZ 85287, USA.*

⁵*Department of Astronomy, Yale University, New Haven, CT 06511*

Submitted to ApJ

ABSTRACT

When a star undergoes core collapse, a vast amount of energy is released in a ~ 10 s long burst of neutrinos of all species. Inverse beta decay in the star’s hydrogen envelope causes an electromagnetic cascade which ultimately results in a flare of gamma rays – an “echo” of the neutrino burst – at the characteristic energy of 0.511 MeV. We study the phenomenology and detectability of this flare. Its luminosity curve is characterized by a fast, seconds-long, rise and an equally fast decline, with a minute- or hour-long plateau in between. For a near-Earth star (distance $D \lesssim 1$ kpc) the echo will be observable at near future gamma ray telescopes with an effective area of 10^3 cm² or larger. Its observation will inform us on the envelope size and composition. In conjunction with the direct detection of the neutrino burst, it will also give information on the neutrino emission away from the line of sight and will enable tests of neutrino propagation effects between the stellar surface and Earth.

Keywords: Core-collapse Supernovae (304), Gamma-ray Astronomy (628), Gamma-ray Burst (629), Neutrino Astronomy(1100), Supernova Neutrinos(1666)

1. INTRODUCTION

A core collapse supernova is the most powerful neutrino emitter known so far. The ~ 10 s-long burst of thermal neutrinos emitted from the outskirts of the collapsed core is the main cooling mechanism, and is a powerful diagnostic tool of the physics that takes place in the very dense and hot region deep inside the star.

Interestingly, one of the best supernova neutrino detectors is the most abundant element in the universe, Hydrogen. Indeed, the process of inverse β decay (IBD), $\bar{\nu}_e + p \rightarrow e^+ + n$, has a relatively large, well known, cross section (Vogel & Beacom 1999; Strumia & Vissani 2003) and, depending on the type of detector, it can

provide information on the energies and arrival times of the individual neutrinos detected. This simple, reliable method has found application in water and liquid scintillator detectors (Scholberg 2012), and it was used in the first and only detection of supernova neutrinos, the burst from SN1987A (Hirata et al. 1987; Bionta et al. 1987; Alekseev et al. 1988). Its evolution has been driven by the need of having larger detector masses; e.g., about $\mathcal{O}(100)$ kt mass of water is needed for high statistics detection of supernovae beyond our galaxy.

The concept of Hydrogen as detector leads to an idea: why not use the vast mass of Hydrogen *in or near the star itself* as detector? This question was first studied several decades ago, when it was observed in Bisnovatyi-Kogan et al. (1975); Ryazhskaya (1999) that inverse beta decay in the hydrogen envelope of a collapsing star leads to a transient signal of positron annihilation ($e^+ + e^- \rightarrow \gamma + \gamma$) signatures, mainly in the form of

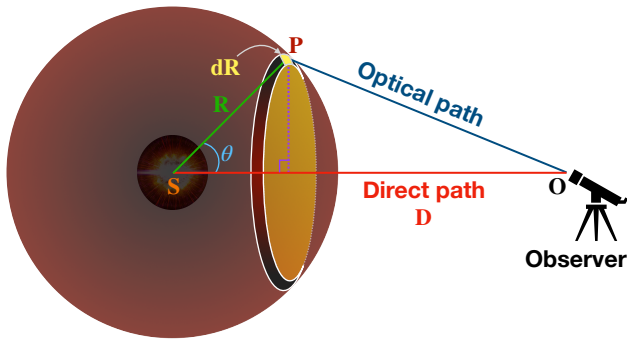


Figure 1. Geometry of a gamma ray echo.

0.511 MeV gamma rays (Lu & Qian 2007)¹. Due to the geometry of the system (Figure 1), these gamma rays arrive at Earth as an *echo*, spread over a characteristic time $\Delta t \sim R/c$ (with R being the star’s radius), relative to the neutrino burst. In those early studies, the predicted luminosity of this echo was considered too low for observation, and therefore this phenomenon was largely ignored since.

In this letter, we present a modern study of the gamma ray echo of a supernova neutrino burst. There are two main elements of novelty. The first is a prediction of the gamma ray light curve, and its dependence on the main parameters. The second is the discussion of the potential of upcoming gamma-ray surveys to observe the echo from nearby core-collapse supernovae, and extract important information from it. With improved, next-generation, gamma ray telescopes like COSI (Tomsick 2021) (already funded), AMEGO (Caputo et al. 2019; Kierans 2020), and AMEGO-X (Caputo et al. 2022), detecting this 511 keV signal will soon be a realistic possibility.

The paper is organized as follows. We discuss the formalism of the gamma ray echo, along with its time-dependent flux in section 2. The detectability of the echo, and relevant backgrounds are discussed in section 3. We summarize and discuss future prospects in section 4.

2. FORMALISM

To fix the ideas, we focus on the case which is most favorable for detection, where the gamma rays originate near the surface of the star, and propagate without absorption to Earth (attenuation will be discussed below). Let’s begin by estimating the total photon flux at Earth. We assume a spherically symmetric star, and model the

flux of $\bar{\nu}_e$ reaching its surface (after flavor conversion, see, e.g. Duan & Kneller 2009 for a review) as having total energy $E_{\nu,tot} = 5 \cdot 10^{52}$ ergs.

The commonly used “alpha spectrum” is assumed for its energy distribution (Keil et al. 2003; Tamborra et al. 2012), with the first two momenta being $\langle E_\nu \rangle = 15$ MeV and $\langle E_\nu^2 \rangle = 293.2$ MeV² (corresponding to the shape parameter $\alpha = 2.3$, where $(1 + \alpha)^{-1} = \langle E_\nu^2 \rangle / \langle E_\nu \rangle^2 - 1$). For simplicity, we use a time-independent spectrum, so the total number of $\bar{\nu}_e$ emitted is, simply, $N_\nu = E_{\nu,tot} / \langle E_\nu \rangle \simeq 2.1 \cdot 10^{57}$. Two cross sections are relevant here: one is the spectrum-averaged IBD cross section, $\langle \sigma_{IBD} \rangle = 2.05 \cdot 10^{-41}$ cm², the other is for the Compton scattering of gamma rays, $\sigma_C = 3 \cdot 10^{-25}$ cm² (Rybicki & Lightman 1986), which is the main channel of photon absorption at the energies of interest (Lu & Qian 2007). As an approximation, we consider that the emerging flux of gamma rays is entirely due to the $\bar{\nu}_e$ that interact in the outermost layer of the star, a very thin shell of width equal to the gamma ray Compton optical depth ($l_C \sim \mathcal{O}(10^9)$ cm, $l_C \ll R$, see Lu & Qian 2007). One can then express the number of positrons produced in this layer, and the corresponding number of gamma rays from positron propagation that leave the star as (Ryazhskaya 1999):

$$N_+ \simeq \frac{Y_p \langle \sigma_{IBD} \rangle}{Y_e \sigma_C} N_\nu \simeq 1.25 \cdot 10^{41} ;$$

$$N_\gamma = \frac{1}{2} \eta_\gamma N_+ \sim N_+ , \quad (1)$$

where $Y_p \sim 1$ and $Y_e \sim 1$ are the proton and electron fractions in the stellar matter; $\eta_\gamma \sim 2$ is the effective number of 0.511 MeV gamma rays produced per positron (see below), and the factor 1/2 accounts for the fact that half of the gamma rays propagates inwards and is absorbed. By symmetry arguments, it follows immediately that the time-integrated photon flux at Earth is ²

$$\Phi_{\gamma,tot} = \frac{N_\gamma}{4\pi D^2} \sim 10^{-3} \text{ cm}^{-2} \left(\frac{D}{\text{kpc}} \right)^{-2} . \quad (2)$$

We estimate the uncertainty on N_+ and N_γ to be about $\sim 50\%$ in either direction due to the uncertainty in the neutrino spectrum parameters.

2.1. Time-dependent gamma ray flux

¹ Other channels were considered, but the most dominant signal was the 0.511 MeV γ -rays.

² Our result is a factor of 4 larger than the one in Lu & Qian (2007). We were unable to trace the origin of the difference; still, the geometric factor $4\pi D^2$ in Equation (2) is substantiated by the extended derivation in Favorite (2016).

To compute the expected time-dependent gamma ray flux and its energy spectrum, it is necessary to consider a specific stellar environment and model the positron propagation in detail. Here we follow the extensive discussion in Lu & Qian (2007), where a precise estimate for η_γ is found. There, the values $Y_p = 0.7$ and $Y_e = 0.85$ are used. It is shown that positron annihilation is the main channel of gamma ray production, dominating over the secondary channel – the emission of 2.22 MeV gamma rays from neutron capture – by roughly two orders of magnitude in flux. For a hydrogen envelope in thermodynamic equilibrium at temperature $T \sim 10^4$ K and density $\rho \sim 10^{-8}$ g cm $^{-3}$, it was found that positron thermalization is – in the vast majority of cases – fast, occurring over a typical time scale of $\sim 10^{-2}$ s, with the excitation of free electrons being the dominant energy loss mechanism. Direct positron annihilation with free electrons is the main absorption process, and the probability that it occurs before thermalization is estimated to be $P_{fa} \simeq 0.1$ (see eq. (53)

in Lu & Qian (2007)). Therefore, roughly a fraction $P \sim 1 - P_{fa} \simeq 0.9$ of all positrons annihilate after thermalization. A more detailed calculation, which includes several other energy loss and absorption processes, and the formation of positronium states, leads to $P \simeq 0.87$ (see fig. 3 and related text in Lu & Qian (2007)). The annihilation of thermalized positrons results in a gamma ray spectrum that is centered at $E_\gamma = 0.511$ MeV, with width (full width at half maximum) $\Delta E_\gamma \simeq 2$ keV. Accounting for the fact that each annihilation produces two photons, we therefore estimate $\eta_\gamma = 2P = 1.74$ which will be used here as reference value.

Let us now describe the expected gamma ray lightcurve at Earth, for a star at distance D , and a given neutrino number luminosity $L_\nu(t) = dN_\nu/dt$. The gamma ray flux at Earth, Φ_γ , is obtained by integrating over the visible surface of the star, and by considering that photons reach the detector with a time delay that increases with their angular distance, θ , from the line of sight (see Figure 1). We find the expression:

$$\begin{aligned} \Phi_\gamma(t, R, D) &= \frac{\eta_\gamma}{8\pi D^2} \frac{Y_p \langle \sigma_{IBD} \rangle}{Y_e \sigma_C} \int_0^1 L_\nu \left(t - \frac{R}{c} (1 - \cos \theta) \right) d(\cos \theta) , \\ &= \frac{\eta_\gamma}{8\pi D^2} \frac{Y_p \langle \sigma_{IBD} \rangle}{Y_e \sigma_C} \int_{-\infty}^{\infty} B(y) L_\nu(t - y) dy , \end{aligned} \quad (3)$$

which is consistent with Equation (1), and where c is the speed of light, and B is a box function normalized to 1: $B(y) = c/R$ for $0 \leq y \leq R/c$, and $B(y) = 0$ elsewhere. The second line of Equation (3) emphasizes that the echo is described by a convolution operation (see, e.g., the formalism in Dwek et al. 2021). Here $t = 0$ is set to be the start of the neutrino burst as observed at Earth.

2.2. Results

Using the expression in Equation 3, the gamma ray flux can be computed for specific scenarios of neutrino emission. For illustration, we model the neutrino luminosity as a truncated exponential:

$$L_\nu(t) = \begin{cases} L_0 e^{-t/\tau} & 0 \leq t \leq t_0 \\ 0 & \text{elsewhere} \end{cases} , \quad (4)$$

where the limit $t_0 \rightarrow +\infty$ (no truncation) well approximates the case of a neutron-star forming collapse, where the proto-neutron star cools smoothly by neutrino emission over several tens of seconds. The case $t_0 \lesssim 1$ s could describe a collapse with direct black-hole formation (failed supernova, see, e.g. O'Connor & Ott 2011;

Pejcha & Thompson 2015; Ertl et al. 2016), for which the neutrino emission is truncated sharply when the neutrosphere falls within the gravitational radius. Here we take $t_0 = 1$ s (for black hole formation) and $\tau = 3$ s. The description in Equation (4) captures the main features of the luminosity curve over a multi-second timescale, which is sufficient for the present scope. We note that fast fluctuations of $L_\nu(t)$ (over a time scale 0.1 s or less) such as those expected in the first second or so of the neutrino burst (Foglizzo 2001; Blondin et al. 2003; Foglizzo 2002) would in any case be smoothed out by the integration in Equation (3), and therefore have a negligible effect on the gamma ray lightcurve.

The result for the case of a neutron-star forming collapse is sufficiently simple, and is given by:

$$\Phi_\gamma(t, R, D) = \Phi_0(R, D) \begin{cases} 0 & t \leq 0 \\ \left(1 - e^{-\frac{t}{\tau}}\right) & 0 < t \leq R/c \\ \left(e^{\frac{R}{c\tau}} - 1\right) e^{-\frac{t}{\tau}} & t > R/c \end{cases} , \quad (5)$$

$$\Phi_0(R, D) = \frac{\eta_\gamma}{8\pi D^2} \frac{Y_p \langle \sigma_{IBD} \rangle}{Y_e \sigma_C} \frac{L_0 c \tau}{R} .$$

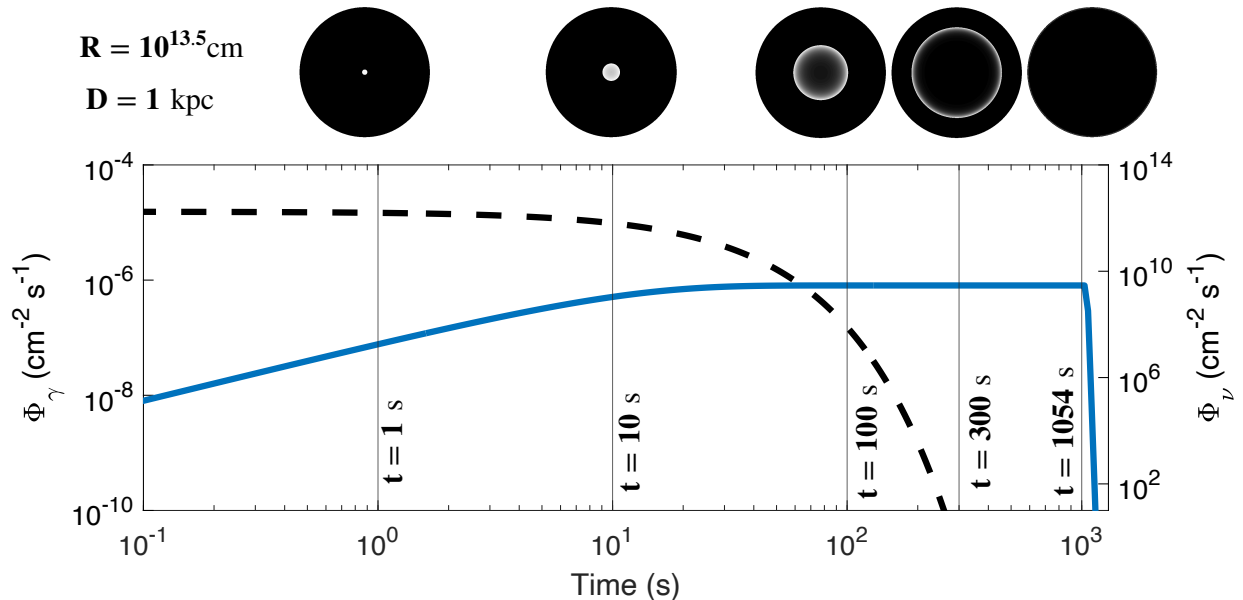


Figure 2. Example of neutrino (dashed, vertical axis on the right) and gamma ray (solid, vertical axis on the left) lightcurves. See legend for the stellar radius and distance to Earth. Included are time snapshots of the star, showing the part that shines in gamma rays as seen by an observer at Earth (regions in white in the black disks).

The results are shown in Figure 2 and 3 (solid curves). The expression in Equation (5) describes the “phases” of the star as seen by an observer at Earth (see illustration in Figure 2): first, there is an increase in flux ($0 \leq t \leq R/c$), when the surface of the star becomes bright in a circle around the line of sight, and the circle expands. After a time comparable with the neutrino emission timescale, $t \sim 3\tau$, the luminosity of the echo has reached a plateau. This behavior describes the phase where the gamma-ray emitting region of the star – as seen at Earth – is made of an expanding annulus where the intensity of emission is at its maximum, whereas the region near the line of sight emits less intensely due to the decline on L_ν . The plateau lasts until $t = R/c$, when the entire visible face of the star has become bright in gamma rays; at later times the star still appears completely illuminated, but the gamma ray flux declines over a timescale $\sim \tau$ because all the points on its surface are receiving a neutrino flux that is past its peak luminosity.

As shown in Equations (3) and (5), and Figure 3, the echo becomes fainter and longer for larger envelope radii; for a reference radius $R = 10^{13.5}$ cm and distance $D = 1$ kpc to the star, we estimate a duration of $R/c \simeq 10^3$ s (approximately 17 minutes) and maximum flux $\Phi_\gamma \sim 10^{-6}$ cm $^{-2}$ s $^{-1}$.

The case of a failed supernova – for which the analytical result is complicated, and will be omitted for simplicity – is described in Figure 3 (dotted lines). Qualitatively, the behavior is similar to the previous case,

with the difference that the transition between phases is sharper, reflecting the sudden drop of L_ν . In this case, an observer at Earth would see a sharp boundary between a fully illuminated annulus and a completely dark circle centered at the line of sight. Note that, by construction, the total energy emitted in neutrinos is the same for the two types of collapses. Therefore, due to the shorter time scale of the emission, for a failed supernova the rise phase of the echo is more luminous and could be more easily observed.

2.3. Attenuation

Let us briefly discuss the attenuation of the emitted gamma rays due to propagation in the circumstellar medium (CSM) and interstellar medium (ISM). The attenuation factor is $\eta_{abs} = \exp(-\int ds \kappa_\nu \rho)$, where κ_ν , and ρ are the monochromatic opacity and density of the medium respectively, and the integral is performed along the line of sight. For simplicity, we approximate the CSM using the radially averaged density and temperature profiles from Georgy et al. (2013), where typical values are in the range: $-29 \lesssim \log(\rho/\text{g/cm}^3) \lesssim -22.5$, $2.5 \lesssim \log(T/\text{K}) \lesssim 8.5$. For these, the 0.511 MeV photon interactions are dominated by Compton scattering (in the Klein-Nishina regime): $\kappa_\nu \approx 0.071$ cm 2 /g. Absorption by atoms and ions is negligible, being most effective at lower energy (see Figure 4, where the corresponding spectral lines are shown). We find that attenuation is practically negligible; for example $\eta_{abs} - 1 \simeq 1.5 \cdot 10^{-6}$

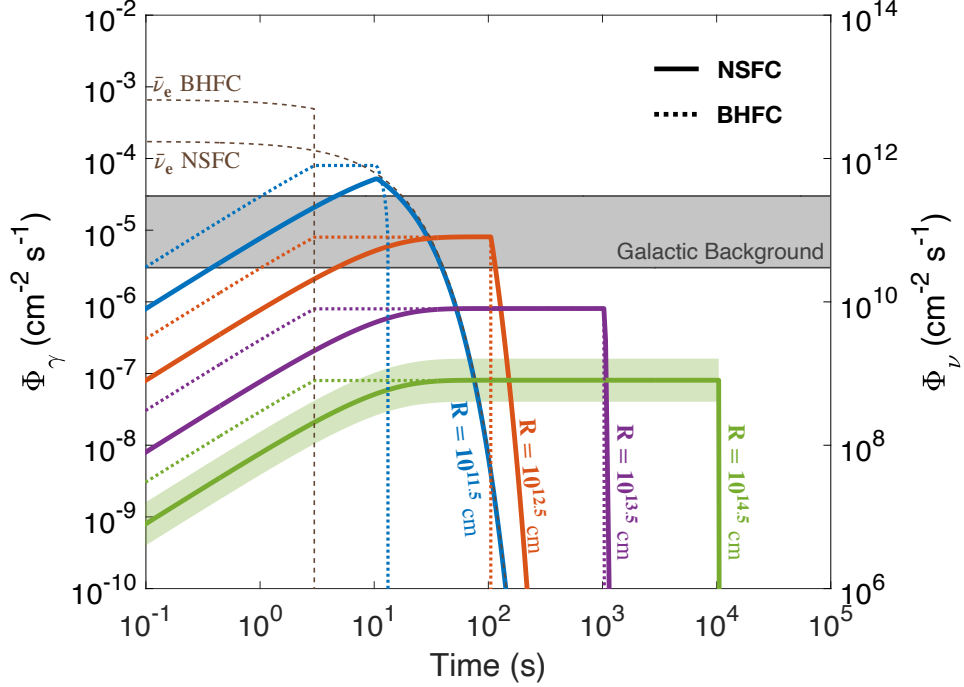


Figure 3. Predicted gamma ray lightcurves for a neutron-star-forming collapse (NSFC, solid lines) and a direct black-hole-forming collapse (BHFC, dotted lines), at distance $D = 1$ kpc and different stellar radii (labels on curves). Dashed: $\bar{\nu}_e$ flux for the two cases (see right vertical axis for scale). For all the results, we used $E_{\nu,tot} = 5 \cdot 10^{52}$ ergs for the total energy emitted in $\bar{\nu}_e$. The galactic background is shown as well. For both signal (one case only, for illustration) and background, the shadings represent the uncertainties discussed in the text.

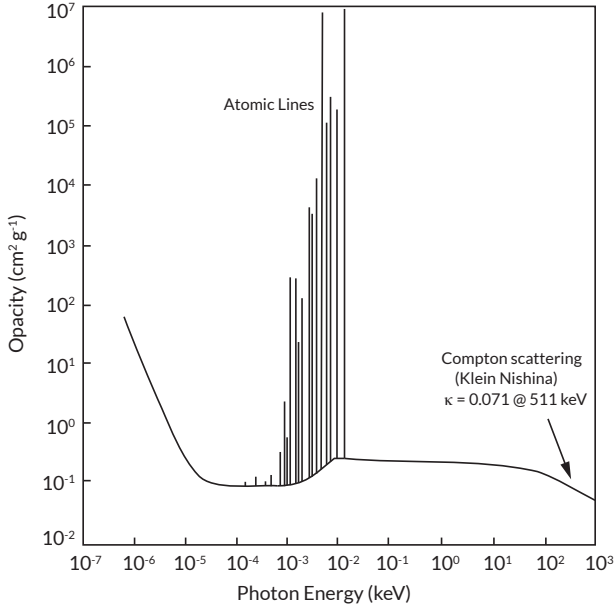


Figure 4. A schematic graph illustrating the opacities of the ISM corresponding to the various values of photon energy. The regime of interest for this work (0.511 MeV) is shown with an arrow.

for a CSM of 15 pc width, and $\eta_{abs} - 1 \simeq 2.2 \cdot 10^{-4}$ for propagation in the ISM over a distance of 1 kpc.

3. DETECTABILITY

In this section, we focus on the detectability of the gamma ray echo and discuss the relevant backgrounds. The echo is detectable *in principle* if it produces at least one photon signal in a detector at Earth: $N_s = A\Phi_{\gamma,tot} \gtrsim 1$, where A is the effective area of the telescope, which we assume to be pointing in the direction of the star (incidence angle $\theta_i = 0$). Using Equation (2), we obtain the detectability condition (for fixed neutrino flux parameters):

$$\left(\frac{A}{10^3 \text{ cm}^2}\right) \left(\frac{D}{\text{kpc}}\right)^{-2} \gtrsim 1. \quad (6)$$

Current or upcoming instrument typically have $A \lesssim 10^2$ cm² (see, e.g, COSI Tomsick 2021 and 511-CAM Shirazi et al. 2023), and would therefore only be able to observe an echo from a very nearby collapse with an exceptionally luminous neutrino emission. In particular, the NASA funded detector COSI has $A > 20$ cm² as design sensitivity at 511 keV, along with a 25% field of view of the sky and an angular resolution of $< 4.1^\circ$. With a factor of 2 improvement on its design specification ($A = 40$ cm²), COSI would be able to see the echo from stars at $D \sim 0.2$ kpc, like supernova candidates Betelgeuse and ϵ Pegasi. For the largest telescopes of

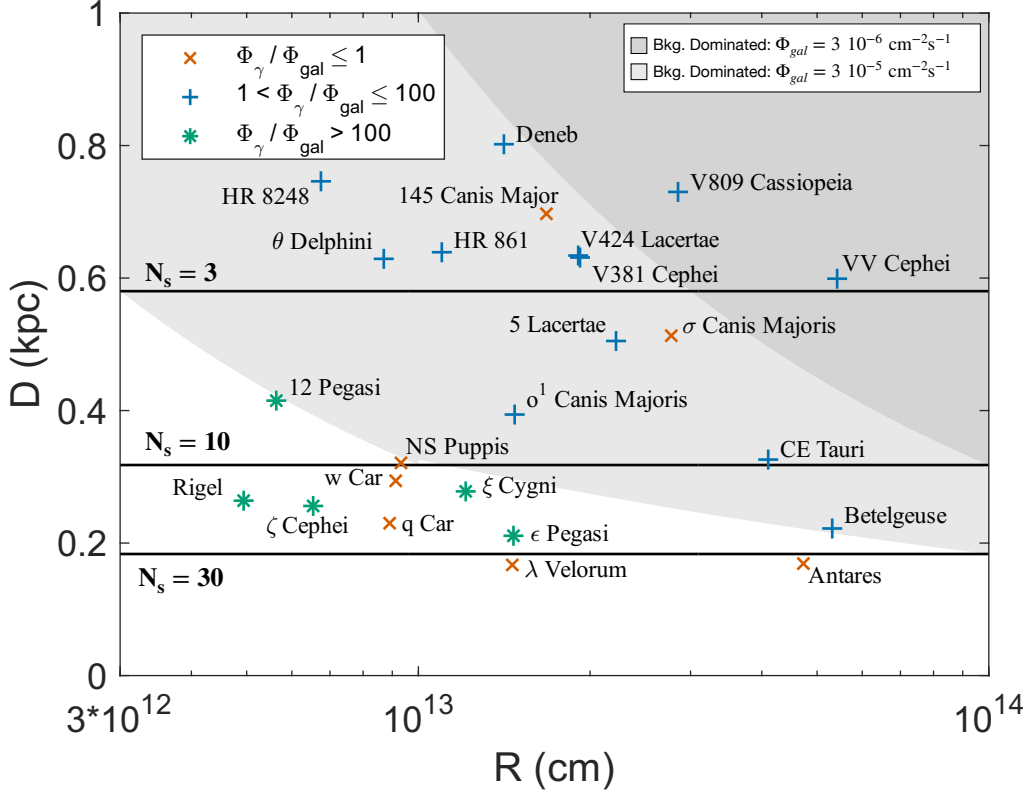


Figure 5. The detectability of the echo depending on the distance, D , and the stellar radius, R , for a telescope with $A = 10^3 \text{ cm}^2$ area. The horizontal (solid) lines correspond to a fixed number of signal events N_s (numbers on curves). The region outside the shaded areas is where the signal can be distinguished from the background (see text), assuming a (fixed) galactic background flux $\Phi_{gal} = 3 \cdot 10^{-6} \text{ cm}^{-2} \text{ s}^{-1}$ (darker shading) and $\Phi_{gal} = 3 \cdot 10^{-5} \text{ cm}^{-2} \text{ s}^{-1}$ (lighter shading) respectively. The markers represent the nearby stars for which the radii are known, and correspond to different intervals of realistic (direction-specific) signal-to-background ratio; see legend and Table 1.

the next generation, AMEGO (Caputo et al. 2019; Kierans 2020) ($A \sim 3 \cdot 10^3 \text{ cm}$), and GECCO ($A \sim 800 \text{ cm}$) (Orlando et al. 2022), the echo might be visible for stars within a radius of 1 kpc or so, where about 31 supernova candidates are located (Mukhopadhyay et al. 2020).

3.1. Backgrounds

Realistically, detection requires the signal to be distinguishable above the relevant backgrounds, mainly the diffuse galactic background at $E_\gamma = 0.511 \text{ MeV}$, which peaks in the direction of the Galactic Center (see, e.g., Diehl 2013; Roland 2016; Diehl et al. 2021; Frontera et al. 2021). We do not consider possible contamination of an echo signal from other nearby sources like gamma ray bursts, other supernovae, supernova remnants, low mass X-ray binaries, and others. Positron annihilation from competing processes in the stellar envelope is unlikely to contribute, as the temperature of the envelope is well below the threshold for thermally producing electron-positron pairs, and positrons from (post-collapse) radionuclides near the core of the star

would be located too deep to affect the echo over its short timescale.

Let us estimate the diffuse galactic background at $E_\gamma = 0.511 \text{ MeV}$. We take the value $d\Phi_{gal}/d\Omega \simeq 3 \cdot 10^{-4} \text{ cm}^{-2} \text{ s}^{-1} \text{ sr}^{-1}$ as a reference for this flux away from the galactic center (see results in Skinner et al. 2015, for galactic latitude and longitude $b = 0^\circ$ and $|l| = 60^\circ$). Taking the published angular resolution of AMEGO, $\delta\theta \simeq 3^\circ$ ³ (corresponding to a solid angle $\delta\Omega = \pi(\delta\theta)^2 \simeq 10^{-2} \text{ sr}$), we obtain a flux $\Phi_{gal} \simeq 3 \cdot 10^{-6} \text{ cm}^{-2} \text{ s}^{-1}$, which is comparable to the maximum value predicted for the echo for $R \gtrsim 10^{13} \text{ cm}$ and $D = 1 \text{ kpc}$ (see Figure 3). This indicates that realistically, a distance below the kpc scale is needed for a robust identification of the echo. A rough criterion for the signal to be detectable above the background is that the number of signal photon counts exceeds the one of the background over the duration of the echo: $N_s/N_B \gtrsim 1$, where

³ Available at AMEGO technical sheet.

$N_B \simeq \Phi_{gal} AR/c^4$. Numerically, we get:

$$\left(\frac{\Phi_{gal}}{3 \cdot 10^{-6} \text{cm}^{-2} \text{s}^{-1}} \right) \left(\frac{D}{1 \text{kpc}} \right)^2 \left(\frac{R}{10^{13} \text{cm}} \right) \lesssim 0.74. \quad (7)$$

If $N_s \gtrsim 10$, one can use the (less stringent) requirement that the signal exceeds a 3σ Gaussian fluctuation of the background: $N_s > 3\sqrt{N_B}$.

3.2. Prospects for detection amongst nearby supernova candidates

Since a detection is possible only for near-Earth collapses, we have examined the known hydrogen-rich supernova candidate stars within a radius of 1 kpc; they are listed in Table 1 (taken from Mukhopadhyay et al. 2020 with some updates, see table caption). For each, we report the estimated distance and radius, the value of Φ_{gal} in the direction of the star and our result for N_s/N_B . The direction-specific Φ_{gal} is evaluated from Skinner et al. (2015) (see Figure 2 there). In the absence of a detailed three dimensional model of the galactic background, the angular separation between the galactic center and the star has been calculated only along the galactic longitude (l), assuming latitude $b = 0$. For stars with angular separation exceeding 90° , we take the fixed value $\Phi_{gal} = 3.0 \cdot 10^{-7} \text{cm}^{-2} \text{s}^{-1}$, which is an overestimate, and therefore leads to conservative conclusions.

The conditions for detectability, Equations (6) and (7) (and its extension to Gaussian statistics, see above), are illustrated in Figure 5, for two fixed values of the galactic background flux, $\Phi_{gal} = 3 \cdot 10^{-6} \text{cm}^{-2} \text{s}^{-1}$ and $\Phi_{gal} = 3 \cdot 10^{-5} \text{cm}^{-2} \text{s}^{-1}$. The candidate stars in Table 1 are shown as well, color coded according to the realistic (direction-specific) signal-to-background ratio given in the Table. From the figure, it appears that the detection of the echo is possible - with a telescope having $A \gtrsim 10^3 \text{cm}$ - for several candidates. Many of them are in a fortunate location, where the galactic background is low. Examples are Betelgeuse and Rigel, for which the angular separation from the galactic center is $\sim 157^\circ$ and $\sim 123^\circ$ respectively, and therefore the background is overestimated. Rigel is also favored by its relatively compact size, $R \simeq 5 \cdot 10^{12} \text{cm}$, which implies a higher peak of the echo flux (see Figure 3). In contrast, Antares - which is similar in distance and radius to Betelgeuse - is disfavored by its proximity to the Galactic Center, which

causes a higher background ($\Phi_{gal} \simeq 2.3 \cdot 10^{-5} \text{cm}^{-2} \text{s}^{-1}$) and lower signal-to-background ratio.

4. DISCUSSION AND FUTURE PROSPECTS

The observation of the gamma ray echo could reveal information that would otherwise be inaccessible. In particular, the echo provides information on the $\bar{\nu}_e$ flux passing through the stellar surface facing the observer. Therefore, the comparison with the detected neutrino burst would test the intensity of the neutrino emission *away from the line of sight*. It would also allow to search for exotic effects that might affect the neutrinos between the star and Earth, like neutrino decay, conversion into sterile states, scattering on Dark Matter, etc. Our predicted gamma ray flux might serve as a reference for searches of gamma-ray-producing effects beyond the Standard Model, like axion-photon conversion (see, e.g. Chattopadhyay et al. 2023 for a related idea). The echo could also provide independent estimates of the progenitor star's features, mainly the radius and envelope composition. Its initial, rising phase could also contribute to early alerts of the collapse, preceding the explosion (or collapse into black hole) of the star.

This work can be extended in many ways, to obtain more realistic predictions. For example, post-main sequence massive stars undergo radial pulsations with periods of 100 – 1000 days (Goldberg et al. 2020), which would change the envelope structure, and therefore influence the lightcurve of the gamma ray echo. One could also use numerical results for the stellar envelope structure and composition and for the neutrino luminosity, that might include deviations from spherical symmetry. Different, more realistic forms of the time profile of the neutrino luminosity could be examined (e.g., a power-law form, see Suwa et al. 2021). Including secondary branches of positron propagation, and the contribution of the layers of the star deeper than the gamma ray optical depth may result in more optimistic predictions for the gamma ray flux. The idea of a gamma ray echo could be extended to other set-ups, for example involving supernova progenitors with Carbon- or Oxygen-rich envelopes - where gamma rays can be produced by neutrino-nucleus scattering - , or envelope-stripped stars where the echo might be due to a detached hydrogen shell (for example, the shell between two companion stars, see, e.g., Pejcha et al. 2022). The latter, however, might give very faint echoes due to their more extended structure (larger R).

In conclusion, we have presented a modern rendering of the idea of supernova neutrinos producing a gamma ray echo. This phenomenon is conceptually interesting, because the neutrinos take the unusual role of being

⁴ For simplicity, here we refer to the case where the signal flux is dominated by the plateau phase, i.e., $R/c \gg 10 \text{s}$, which is realized for the nearby stars considered here (Table 1). In this case the condition $N_s/N_B \gtrsim 1$ is well approximated by $\Phi_\gamma/\Phi_{gal} \gtrsim 1$, with Φ_γ being the flux at the plateau.

the source of an electromagnetic signal, and is also attractive as a realistic target of observation for future large gamma ray telescopes with sub-MeV capability. It adds another facet to the very rich landscape of multi-messenger astronomy.

1 We thank Christopher Fontes from Los Alamos National
 2 Laboratory for his help in determining the monochrom-
 3 atic opacity for 0.511 MeV γ -rays. We are grateful
 4 to Regina Caputo, Yong-Zhong Qian and Yudai Suwa
 5 for useful discussions. We also thank Carolyn A. Kier-
 6 ans for providing us with the effective area for COSI.
 7 CL acknowledges support from the NSF grant PHY-
 8 2309973, and from the National Astronomical Observa-
 9 tory of Japan, where part of this work was conducted.
 10 M. M. is supported by NSF Grant No. AST-2108466.
 11 M. M. also acknowledges support from the Institute for
 12 Gravitation and the Cosmos (IGC) Postdoctoral Fel-
 13 lowship. FXT and EF acknowledge support from NSF
 14 under grant 2154339 entitled "Neutrino Emission From
 15 Stars".

REFERENCES

- Alekseev, E. N., Alekseeva, L. N., Krivosheina, I. V., & Volchenko, V. I. 1988, *Phys. Lett. B*, 205, 209, doi: [10.1016/0370-2693\(88\)91651-6](https://doi.org/10.1016/0370-2693(88)91651-6)
- Baines, E. K., Armstrong, J. T., Schmitt, H. R., et al. 2018, *The Astronomical Journal*, 155, 30, doi: [10.3847/1538-3881/aa9d8b](https://doi.org/10.3847/1538-3881/aa9d8b)
- Bionta, R. M., et al. 1987, *Phys. Rev. Lett.*, 58, 1494, doi: [10.1103/PhysRevLett.58.1494](https://doi.org/10.1103/PhysRevLett.58.1494)
- Bisnovatyi-Kogan, G. S., Imshennik, V. S., Nadyozhin, D. K., & Chechetkin, V. M. 1975, *Astrophys. Space Sci.*, 35, 23, doi: [10.1007/BF00644821](https://doi.org/10.1007/BF00644821)
- Blondin, J. M., Mezzacappa, A., & DeMarino, C. 2003, *Astrophys. J.*, 584, 971, doi: [10.1086/345812](https://doi.org/10.1086/345812)
- Caputo, R., et al. 2019. <https://arxiv.org/abs/1907.07558>
- . 2022, *J. Astron. Telesc. Instrum. Syst.*, 8, 044003, doi: [10.1117/1.JATIS.8.4.044003](https://doi.org/10.1117/1.JATIS.8.4.044003)
- Carpenter, K. G., Robinson, R. D., Harper, G. M., et al. 1999, *Astrophys. J.*, 521, 382, doi: [10.1086/307520](https://doi.org/10.1086/307520)
- Chattopadhyay, D. S., Dasgupta, B., Dighe, A., & Narang, M. 2023. <https://arxiv.org/abs/2311.14298>
- Diehl, R. 2013, *The Astronomical Review*, 8, 19, doi: [10.1080/21672857.2013.11519722](https://doi.org/10.1080/21672857.2013.11519722)
- Diehl, R., Lugaro, M., Heger, A., et al. 2021, *PASA*, 38, e062, doi: [10.1017/pasa.2021.48](https://doi.org/10.1017/pasa.2021.48)
- Duan, H., & Kneller, J. P. 2009, *J. Phys. G*, 36, 113201, doi: [10.1088/0954-3899/36/11/113201](https://doi.org/10.1088/0954-3899/36/11/113201)
- Dwek, E., Sarangi, A., Arendt, R. G., et al. 2021, *Astrophys. J.*, 917, 84, doi: [10.3847/1538-4357/ac09ea](https://doi.org/10.3847/1538-4357/ac09ea)
- Ertl, T., Janka, H. T., Woosley, S. E., Sukhbold, T., & Ugliano, M. 2016, *Astrophys. J.*, 818, 124, doi: [10.3847/0004-637X/818/2/124](https://doi.org/10.3847/0004-637X/818/2/124)
- Favorite, J. A. 2016, *Nuclear Instruments and Methods in Physics Research Section A: Accelerators, Spectrometers, Detectors and Associated Equipment*, 813, 29, doi: <https://doi.org/10.1016/j.nima.2015.12.060>
- Foglizzo, T. 2001, *Astron. Astrophys.*, 368, 311, doi: [10.1051/0004-6361:20000506](https://doi.org/10.1051/0004-6361:20000506)
- . 2002, *Astron. Astrophys.*, 392, 353, doi: [10.1051/0004-6361:20020912](https://doi.org/10.1051/0004-6361:20020912)
- Frontera, F., Virgili, E., Guidorzi, C., et al. 2021, *Experimental Astronomy*, 51, 1175, doi: [10.1007/s10686-021-09727-7](https://doi.org/10.1007/s10686-021-09727-7)
- Gaia Collaboration. 2018, *Astron. Astrophys.*, 616, A1, doi: [10.1051/0004-6361/201833051](https://doi.org/10.1051/0004-6361/201833051)
- Georgy, C., Walder, R., Folini, D., et al. 2013, *Astron. Astrophys.*, 559, A69, doi: [10.1051/0004-6361/201321226](https://doi.org/10.1051/0004-6361/201321226)
- Goldberg, J. A., Bildsten, L., & Paxton, B. 2020, *ApJ*, 891, 15, doi: [10.3847/1538-4357/ab7205](https://doi.org/10.3847/1538-4357/ab7205)
- Hirata, K., et al. 1987, *Phys. Rev. Lett.*, 58, 1490, doi: [10.1103/PhysRevLett.58.1490](https://doi.org/10.1103/PhysRevLett.58.1490)
- Joyce, M., Leung, S.-C., Molnár, L., et al. 2020, *Astrophys. J.*, 902, 63, doi: [10.3847/1538-4357/abb8db](https://doi.org/10.3847/1538-4357/abb8db)
- Kallinger, T., Beck, P. G., Hekker, S., et al. 2019, *Astron. Astrophys.*, 624, A35, doi: [10.1051/0004-6361/201834514](https://doi.org/10.1051/0004-6361/201834514)
- Keil, M. T., Raffelt, G. G., & Janka, H.-T. 2003, *Astrophys. J.*, 590, 971, doi: [10.1086/375130](https://doi.org/10.1086/375130)
- Kierans, C. A. 2020, *Proc. SPIE Int. Soc. Opt. Eng.*, 11444, 1144431, doi: [10.1117/12.2562352](https://doi.org/10.1117/12.2562352)
- Levesque, E. M., Massey, P., Olsen, K. A. G., et al. 2005, *Astrophys. J.*, 628, 973, doi: [10.1086/430901](https://doi.org/10.1086/430901)
- Lu, Y., & Qian, Y.-Z. 2007, *Phys. Rev. D*, 76, 103002, doi: [10.1103/PhysRevD.76.103002](https://doi.org/10.1103/PhysRevD.76.103002)

Table 1. Nearby red and blue supergiants and their estimated radii, distances and positions; adapted from Mukhopadhyay et al. (2020). Also given are the angular separation from the galactic center (along l , assuming $b = 0$), the associated 511 keV galactic background, and the predicted signal-to-background ratio. We only list stars to which our scenario applies, namely, stars that have a hydrogen envelope and for which the radius R is known.

Common Name	D (in kpc)	R ($\times 10^{13}$ cm)	RA	Dec	l Sep.	Φ_{gal} ($\text{cm}^{-2}\text{s}^{-1}$)	N_s/N_B
λ Velorum	0.167 ± 0.003	1.46 ^a	09:07:59.76	-43:25:57.3	2.61°	8.64×10^{-5}	0.732
Antares/ α Scorpii	0.169 ± 0.030	4.73 ^b	16:29:24.46	-26:25:55.2	14.94°	1.97×10^{-5}	0.968
ϵ Pegasi	0.211 ± 0.006	1.47 ^c	21:44:11.16	+09:52:30.0	148.76°	2.58×10^{-7}	1.53×10^2
Betelgeuse	0.222 ± 0.040	5.32 ^d	05:55:10.31	+07:24:25.4	157.43°	2.58×10^{-7}	38.1
q Car/V337 Car	0.230 ± 0.020	0.890 ^e	10:17:04.98	-61:19:56.3	2.95°	8.30×10^{-5}	0.659
ζ Cephei	0.256 ± 0.006	0.654 ^f	22:10:51.28	+58:12:04.5	178.74°	2.58×10^{-7}	2.33×10^2
Rigel/ β Orion	0.264 ± 0.024	0.494 ^g	05:14:32.27	-08:12:05.90	122.61°	2.58×10^{-7}	2.90×10^2
ξ Cygni	0.278 ± 0.029	1.21 ^f	21:04:55.86	+43:55:40.3	178.05°	2.58×10^{-7}	1.07×10^2
w Car/V520 Car	0.294 ± 0.023	0.913 ^h	10:43:32.29	-60:33:59.8	1.09°	1.11×10^{-4}	0.296
NS Puppis	0.321 ± 0.032	0.932 ^f	08:11:21.49	-39:37:06.8	3.50°	7.84×10^{-5}	0.342
CE Tauri/119 Tauri	0.326 ± 0.070	4.10 ⁱ	05:32:12.75	+18:35:39.2	167.71°	2.58×10^{-7}	22.9
σ^1 Canis Majoris	0.394 ± 0.052	1.47 ^f	06:54:07.95	-24:11:03.2	22.79°	5.49×10^{-6}	2.05
12 Pegasi	0.415 ± 0.031	0.564 ^f	21:46:04.36	+22:56:56.0	159.50°	2.58×10^{-7}	1.03×10^2
5 Lacertae	0.505 ± 0.046	2.22 ^j	22:29:31.82	+47:42:24.8	173.34°	2.58×10^{-7}	17.6
σ Canis Majoris	0.513 ± 0.108	2.78 ^f	07:01:43.15	-27:56:05.4	19.24°	9.39×10^{-6}	0.376
VV Cephei	0.599 ± 0.083	5.42 ^j	21:56:39.14	+63:37:32.0	174.34°	2.58×10^{-7}	5.13
θ Delphini	0.629 ± 0.029	0.870 ^f	20:38:43.99	+13:18:54.4	157.15°	2.58×10^{-7}	29.0
V381 Cephei	0.631 ± 0.086	1.92 ^j	21:19:15.69	+58:37:24.6	174.68°	2.58×10^{-7}	13.0
V424 Lacertae	0.634 ± 0.075	1.91 ^k	22:56:26.00	+49:44:00.8	173.30°	2.58×10^{-7}	13.0
HR 861	0.639 ± 0.039	1.10 ^l	02:56:24.65	+64:19:56.8	176.43°	2.58×10^{-7}	22.2
145 Canis Major	0.697 ± 0.078	1.68 ^h	07:16:36.83	-23:18:56.1	10.26°	3.99×10^{-5}	0.079
V809 Cassiopeia	0.730 ± 0.074	2.85 ^m	23:19:23.77	+62:44:23.2	178.76°	2.58×10^{-7}	6.56
HR 8248	0.746 ± 0.039	0.675 ^l	21:33:17.88	+45:51:14.5	176.30°	2.58×10^{-7}	26.6
Deneb/ α Cygni	0.802 ± 0.066	1.41 ⁿ	20:41:25.9	+45:16:49.0	178.15°	2.58×10^{-7}	11.0

NOTE— ^aCarpenter et al. (1999), ^bOhnaka et al. (2013), ^cStock et al. (2018), ^dJoyce et al. (2020), ^eKallinger et al. (2019), ^fMessineo & Brown (2019), ^gPrzybilla et al. (2006); Moravveji et al. (2012), ^hGaia Collaboration (2018), ⁱMontargès et al. (2018), ^jBaines et al. (2018), ^kNorris (2019), ^lvan Belle et al. (2009), ^mLevesque et al. (2005), ⁿSchiller & Przybilla (2008).

Messineo, M., & Brown, A. G. A. 2019, The Astronomical Journal, 158, 20, doi: [10.3847/1538-3881/ab1cbd](https://doi.org/10.3847/1538-3881/ab1cbd)

Montargès, M., Norris, R., Chiavassa, A., et al. 2018, Astron. Astrophys., 614, A12, doi: [10.1051/0004-6361/201731471](https://doi.org/10.1051/0004-6361/201731471)

Moravveji, E., Guinan, E. F., Shultz, M., Williamson, M. H., & Moya, A. 2012, Astrophys. J., 747, 108, doi: [10.1088/0004-637X/747/2/108](https://doi.org/10.1088/0004-637X/747/2/108)

Mukhopadhyay, M., Lunardini, C., Timmes, F. X., & Zuber, K. 2020, Astrophys. J., 899, 153, doi: [10.3847/1538-4357/ab99a6](https://doi.org/10.3847/1538-4357/ab99a6)

Norris, R. P. 2019, PhD thesis, Georgia State University, doi: <https://doi.org/10.57709/15009706>

O'Connor, E., & Ott, C. D. 2011, Astrophys. J., 730, 70, doi: [10.1088/0004-637X/730/2/70](https://doi.org/10.1088/0004-637X/730/2/70)

Ohnaka, K., Hofmann, K. H., Schertl, D., et al. 2013, Astron. Astrophys., 555, A24, doi: [10.1051/0004-6361/201321063](https://doi.org/10.1051/0004-6361/201321063)

Orlando, E., et al. 2022, JCAP, 07, 036, doi: [10.1088/1475-7516/2022/07/036](https://doi.org/10.1088/1475-7516/2022/07/036)

Pejcha, O., Calderón, D., & Kurfurst, P. 2022, Mon. Not. Roy. Astron. Soc., 510, 3276, doi: [10.1093/mnras/stab3729](https://doi.org/10.1093/mnras/stab3729)

Pejcha, O., & Thompson, T. A. 2015, Astrophys. J., 801, 90, doi: [10.1088/0004-637X/801/2/90](https://doi.org/10.1088/0004-637X/801/2/90)

- Przybilla, N., Butler, K., Becker, S. R., & Kudritzki, R. P. 2006, *Astron. Astrophys.*, 445, 1099, doi: [10.1051/0004-6361:20053832](https://doi.org/10.1051/0004-6361:20053832)
- Roland, D. 2016, in *Journal of Physics Conference Series*, Vol. 703, *Journal of Physics Conference Series*, 012001, doi: [10.1088/1742-6596/703/1/012001](https://doi.org/10.1088/1742-6596/703/1/012001)
- Ryazhskaya, O. G. 1999, *Nuovo Cimento C Geophysics Space Physics C*, 22C, 115. <https://ui.adsabs.harvard.edu/abs/1999NCimC..22..115R>
- Rybicki, G. B., & Lightman, A. P. 1986, *Radiative Processes in Astrophysics*
- Schiller, F., & Przybilla, N. 2008, *Astron. Astrophys.*, 479, 849, doi: [10.1051/0004-6361:20078590](https://doi.org/10.1051/0004-6361:20078590)
- Scholberg, K. 2012, *Ann. Rev. Nucl. Part. Sci.*, 62, 81, doi: [10.1146/annurev-nucl-102711-095006](https://doi.org/10.1146/annurev-nucl-102711-095006)
- Shirazi, F., et al. 2023, *J. Astron. Telesc. Instrum. Syst.*, 9, 024006, doi: [10.1117/1.JATIS.9.2.024006](https://doi.org/10.1117/1.JATIS.9.2.024006)
- Skinner, G., Diehl, R., Zhang, X.-L., Bouchet, L., & Jean, P. 2015, *PoS, Integral2014*, 054, doi: [10.22323/1.228.0054](https://doi.org/10.22323/1.228.0054)
- Stock, S., Reffert, S., & Quirrenbach, A. 2018, *VizieR Online Data Catalog, J/A+A/616/A33*, doi: [10.26093/cds/vizie.36160033](https://doi.org/10.26093/cds/vizie.36160033)
- Strumia, A., & Vissani, F. 2003, *Phys. Lett. B*, 564, 42, doi: [10.1016/S0370-2693\(03\)00616-6](https://doi.org/10.1016/S0370-2693(03)00616-6)
- Suwa, Y., Harada, A., Nakazato, K., & Sumiyoshi, K. 2021, *PTEP*, 2021, 013E01, doi: [10.1093/ptep/ptaa154](https://doi.org/10.1093/ptep/ptaa154)
- Tamborra, I., Muller, B., Hudepohl, L., Janka, H.-T., & Raffelt, G. 2012, *Phys. Rev. D*, 86, 125031, doi: [10.1103/PhysRevD.86.125031](https://doi.org/10.1103/PhysRevD.86.125031)
- Tomsick, J. A. 2021, *PoS, ICRC2021*, 652, doi: [10.22323/1.395.0652](https://doi.org/10.22323/1.395.0652)
- van Belle, G. T., Creech-Eakman, M. J., & Hart, A. 2009, *Mon. Not. Roy. Astron. Soc.*, 394, 1925, doi: [10.1111/j.1365-2966.2008.14146.x](https://doi.org/10.1111/j.1365-2966.2008.14146.x)
- Vogel, P., & Beacom, J. F. 1999, *Phys. Rev. D*, 60, 053003, doi: [10.1103/PhysRevD.60.053003](https://doi.org/10.1103/PhysRevD.60.053003)